Rethinking Coherent Diffraction Instruments for High Brightness Sources

Yanwen Sun[1], Haoyuan Li[2] and Paul H. Fuoss[1*]

[1] LCLS, SLAC National Accelerator Laboratory, Menlo Park, CA, United States
[2] Mechanical Engineering Dept., Stanford University, Stanford, CA, United States

[*]E-mail: fuoss@slac.stanford.edu

Abstract. Over the past two decades, exceptional progress has been made providing coherent x-ray beams at both high-brightness synchrotron sources and x-ray free electron lasers (XFEL). The availability of these coherent x-rays has led to a surge in instruments that exploit x-ray coherence for either x-ray photon correlation spectroscopy (XPCS) or coherent diffraction imaging (CDI). A key to these techniques has been to resolve, or at least nearly resolve, the speckles associated with the scattering from structural disorder. Given practical limits on detector pixel size, this requires long sample-to-detector distances. This paper presents numerical simulations of an instrument that can efficiently provide a long sample-detector distance while maintaining the ability to rapidly set momentum transfer by inserting crystals with different order in the incident beam, thus changing in incident direction instead of moving the detector.

1. Introduction

The last decade has seen enormous progress in the production of bright x-ray beams. The multi-bend achromat storage ring concept pioneered by MAX-IV, the upgrades of the ESRF and the Advanced Photon Source (APS) has led to remarkable improvements in storage ring performance [1]. The parallel development of X-ray Free Electron Lasers (XFEL) produced hard x-rays beams (photon energies up to 24 keV) with full transverse coherence, exceptionally short x-ray pulses, and extremely high peak intensities [2].

With these new sources has come the opportunity to perform qualitatively new experiments that use coherent scattering techniques to generate high resolution x-ray images with phase-retrieval techniques, and measure dynamics with techniques such X-ray Photon Correlation Spectroscopy (XPCS) [3]. While early coherent x-ray scattering experiments utilized x-ray energies around 8-10 keV, Grübel and coworkers predicted that increasing the x-ray photon energy would greatly expand the range of materials that could be practically studied [4].

In particular, the maximum signal at a particular momentum transfer ($Q = \frac{4\pi sin\theta}{\lambda}$ where λ is the photon wavelength and 2θ is the scattering angle) is optimized for a path length through the sample of $t_0 = 1/\mu$ where μ is the sample's x-ray absorption length. Also, for a given maximum tolerable x-ray intensity, the overall signal is proportional to the illuminated area of the sample. These driving forces, thicker samples and bigger beams, lead to smaller speckles. Assuming a transversely Gaussian beam of width w (rms) interacting with a sample with parallel faces and thickness t, the 3D speckle volume in the reciprocal space is given by the Fourier transform of the

Table 1. Approximate speckle sizes for three different materials for two different photon energies and momentum transfers. The thickness is chosen to be the absorption length ($1/\mu$) and the beam diameter is 20 μm. The angular divergences (S_w, S_t and S_r) are given in microradians.

Material	Photon Energy (keV)	Absorption Length (μm)	S_w	S_t	$Q = 0.1$Å^{-1} S_r	L (m)	$Q = 2.0$Å^{-1} S_r	L(m)
C_3H_6	10	5741	3.97	0.0034	1.56	48	0.09	862
	20	30500	1.98	0.0003	0.32	236	0.02	4640
Aluminum	10	150	3.97	1.29	3.96	19	2.64	28
	20	1168	1.98	0.08	1.93	39	0.42	182
Iron	10	7	3.97	26.10	3.97	19	4.29	18
	20	51	1.98	1.90	1.97	38	1.98	38

diffraction volume $\approx 2w \times 2w \times t_0$ [5]. Thus, the angular transverse and longitudinal speckle sizes ($1/e^2$ diameter) are:

$$S_w = 2\lambda/(\pi w) \approx 0.64\lambda/w$$

and

$$S_t = 2\sqrt{6}\lambda/(t_0\pi) \approx 1.56\lambda/t_0$$

respectively. For scattering at finite Q, S_w and S_t are mixed in the plane of scattering leading to an effective pixel size of:

$$S_r = \frac{S_w S_t}{\sqrt{S_t^2 \cos^2 2\theta + S_w^2 \sin^2 2\theta}}$$

To give a sense of scale, the speckle divergences are given in Table 1 for a variety of materials and photon energies.

The speckle divergence implies, for a detector with a pixel size D_{pixel}, that the required distance from sample to detector L is of order $L = D_{pixel}/S_r$. Using the divergences given in Table 1 and a typical pixel size of 75 μm, the sample to detector distance should range from ≈18 meters to over a kilometer, distances that are challenging to unobtainable using current approaches.

Practical considerations typically restrict diffraction arms to lengths of roughly 8 meters due to space constraints (an eight-meter arm moving over 50° requires ≈45 m^2 of floor space) and challenges with precision motion. Since experimental designs require a 4 megapixel detector recording data at >30,000 frames per second, sensor and on-detector processing electronics require substantial and sophisticated cooling. Reading out and pre-processing the detector's 3.6 gigabytes/second of data requires sophisticated programmable logic arrays, graphic processors, and computers that are connected to the detector through high-capacity parallel channels. Including the massive scale of the arm and the complexity of the detector, it can take several hours to change the diffraction angle at existing instruments. These challenges associated with a moving arm have limited the widespread use of coherent x-ray scattering techniques and slowed scientific progress, particularly in XPCS.

For coherent scattering small angles (C-SAXS) where the detector remains at a small angle, a new approach uses a very large, stationary vacuum chamber contain the detector, for example the

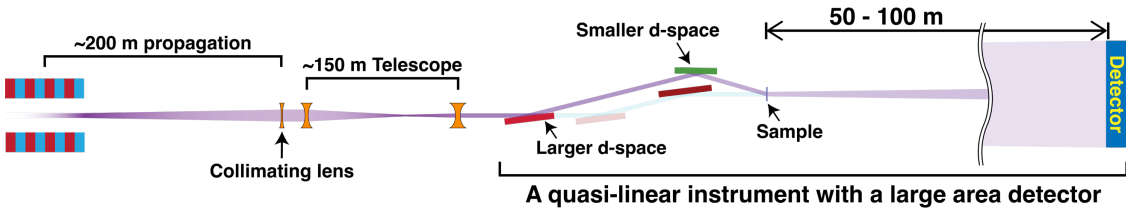

Figure 1. The quasi-linear instrument concept uses mis-matched reflections to get a non-zero scattering angle (momentum transfer). In this approach, the x-ray beam diffracts first from a crystal and then either from a second crystal back parallel to the original beam or a second crystal (green) with a smaller d-spacing back towards the original path. Different crystal pairs allow for rapid switching between different Q's.

CSSI instrument at the APS [6]. This paper describes a novel approach to x-ray scattering instruments that will allow the use of such a large detector chamber, simplified cabling, processing and cooling while still covering a large range of Q.

2. The Quasi-Linear Instrument

The basic instrument concept is shown in Figure 1. The incident x-ray beam is first deflected horizontally using, for example, a C* 400 reflection. If a second C* 400 reflection was used, a beam parallel to the original x-ray beam path would be created. However, if a crystal reflection with a different d-spacing *(e.g.,* a Si 440*)* is used, a non-zero momentum transfer Q can be obtained. In particular, the incident angle on sample is twice the difference between the Bragg angles of the two crystal reflections $\theta_{1(2)}$ with :

$$2\theta = 2\theta_2 - 2\theta_1 = 2\arcsin\frac{\lambda}{2d_2} - 2\arcsin\frac{\lambda}{2d_1}$$

Here d_1 and d_2 are the lattice spacing for the two reflections. Since the detector is mounted on a beam path parallel to the incident beam, this 2θ corresponds to the measured scattering angles.

Using a combination of a C* 400 reflection for the first crystal and a variety of silicon and germanium reflections, an almost continuous Q coverage can be achieved. Figure 2 displays the available Q values and the bandwidth of common crystal-pair combination. For Q's between the discrete points shown, the diffraction peak will move laterally on the detector. As shown in the inset, the typical 2θ difference between adjacent reflections is less than 0.8° and can be reduced to less than 0.4° by using a combination of first crystals. Thus, continuous coverage of reciprocal space can be achieved if the detector subtends 1° (or can be moved a small distance in the scattering plane). For a 60-meter sample to detector distance and using the current 75 μm pixel size, a detector with 12288×4096 (50 MPixels) would provide continuous coverage. Alternatively, a relatively small motion of ≈300 mm with a standard large detector would be adequate.

To quantitatively determine the expected performance of a quasi-linear instrument (QLI), we calculate the ideal speckle contrast using two different approaches. Both approaches start with Pussey and Sutton's derivations of the coherence factor [7,8]. In the Fraunhofer limit, the speckle visibility can be calculated by a double integration of mutual coherence function over the illuminated sample volume V.

$$\beta(\mathrm{Q}) = \frac{1}{V^2\langle|E|^2\rangle^2}\int_V d\boldsymbol{r_1}\int_V d\boldsymbol{r_2}\left|\Gamma\left(\boldsymbol{r_1^{\perp}}, \boldsymbol{r_2^{\perp}}, \frac{\cdot(\boldsymbol{r_2}-\boldsymbol{r_1})}{ck_0}\right)\right|^2$$

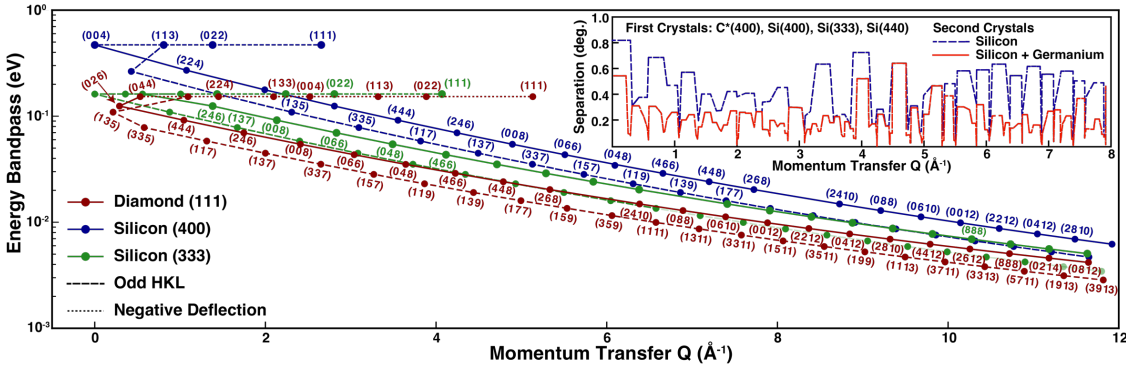

Figure 2. Calculation of Q coverage at 20 keV. (a) Available Q values and the corresponding bandwidths of the output beam at 20 keV considering silicon as the second crystal. Not all of the reflections are labelled since the sequence is the same for each first crystal. Solid and dashed lines connect the even and odd Miller indices respectively. (b) The inset shows the maximum of the angular separation to the adjacent reflections, divided by two, for each crystal choice. The two curves are for a C* 400 and a combination of three silicon reflections.

Here Q is the momentum transfer, c is the speed of light, k_0 is the photon wavevector, $\boldsymbol{r}^{\perp}$ represents the position vector components perpendicular to the beam propagation direction, and Γ is the mutual coherence function introduced by Mandel and Wolf [9]:

$$\Gamma(\boldsymbol{r_1}, \boldsymbol{r_2}, \tau) = \langle E^*(\boldsymbol{r_1}, t) E(\boldsymbol{r_2}, t+\tau) \rangle_t$$

Using approximations given by Sutton [5], Figure 3 shows a comparison of contrast for two different detector distances (6 m and 60 m) as a function of beam size versus sample thickness. Clearly, there is significant contrast gain at 60 meters with usable contrast over a wide range of values. Figure 4 shows the approximate contrast for a conceptual QLI for each of the Q values in Fig. 3 utilizing a C^* 400 first reflection. Of particular interest is the bandwidth decrease at higher Q that provides the needed coherence length to maintain a relatively constant contrast across a wide range of Q's.

While useful for exploring the general performance of the QLI, the approximate approach used in Figs. 3 & 4 ignores many of the aberrations and complications associated with using a SASE beam at an XFEL. Thus, we are pursuing a more complete but much more computationally intensive simulations using the National Energy Research Scientific Computing Center (NERSC). As in the Gaussian case, the calculation is performed at a photon energy of 20 keV and with a source beam waist of 40 μm. Since there are significant fluctuations in a SASE spectrum, 100 pulses were calculated using Genesis 1.3 [10] and then propagated through the optics shown in Fig. 1 Of those

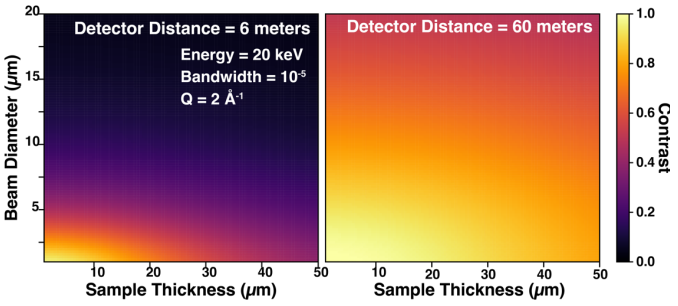

Figure 3. Comparison of the approximate contrast calculated using a transversely coherent x-ray beam for different sample thicknesses and slit sizes for two different detector distances.

pulses, 32 had a contrast above 0.50, 63 above 0.45 and 87 were above 0.40. The images in Fig. 5 are from a typical SASE pulse in the middle of the upper 60% of the distribution and show a weak second mode (see arrows). For a few pulses, there were two modes of roughly comparable intensity that resulted in contrasts as low as 0.24.

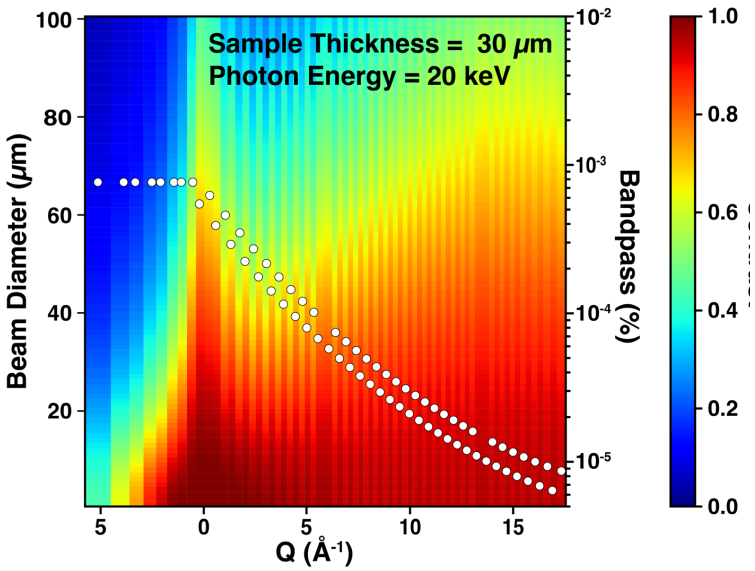

Figure 4. The approximate contrast and bandpass calculated for the silicon reflections in Figure 2 using a C* (400) first reflection.

Discussion

By eliminating the need to swing the diffraction arm, a much longer sample to detector distance is feasible with a quasi-linear instrument while minimizing the constraints on experimental space and costs. Inserting crystals rather than moving a long diffractometer arm allows for rapid changes in momentum transfer. Since the detector does not move, the practical challenge of using large x-ray detectors with 10's-100's of megapixels and the computation demands from high data rates can be more easily met.

While this paper has focused on reciprocal space coherent scattering, we note that a feature of the QLI is the relative ease that x-ray optics can be positioned to image the diffracted beam. An example would be full field x-ray microscope that typically uses an x-ray lens placed close to the sample. The magnification M is then given by $M \approx L_{SL}/L_{LD}$ where L_{SL} is the sample to lens distance and L_{LD} is the lens to detector distance. For this application, the QLI provides for a high magnification and the ability to rapidly change the imaging condition (e.g., by shifting to a different Bragg condition).

We note, however, that increasing the size of the beam and thickness of the sample only modestly increases the count rate per detector pixel since the resultant speckles have a smaller angular

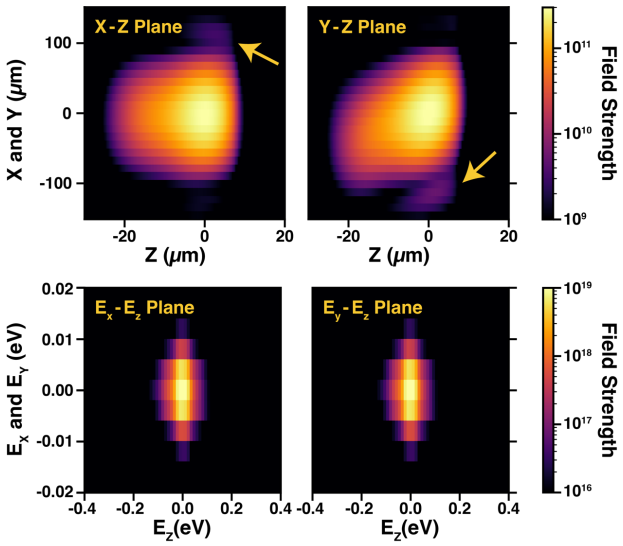

Figure 5. Slices through the focus of a typical SASE pulse after transmission through the quasi-linear instrument. The calculated contrast is 0.52. The arrows point to two locations where a second mode is being transmitted to the focus. For a few pulses the resultant mode pattern is complex and a low contrast (<0.25) is observed.

divergence. However, the signal to noise increases significantly as $\sqrt{N}$ where N is the number of measured speckles.

In conclusion, we propose that a quasi-linear instrument (QLI) can make valuable contributions to coherent scattering and imaging experiments utilizing the spectral brightness of the FEL sources and possibly fourth generation synchrotron sources. We estimate that a QLI would bring at least an order of magnitude increase to the SNR in XPCS measurements and facilitate its application to studies of a wide range of material systems down to the fastest relevant timescales.

Acknowledgements

We appreciate many detailed and helpful discussions with Mark Sutton. This work was supported by the U.S. Department of Energy, Office of Science, Office of Basic Energy Sciences under Contract No. DE-AC02-76SF00515. Work by H.L. was supported by U.S. Department of Energy, Office of Science under DOE (BES) Awards DE-SC0022222. This research used resources of the National Energy Research Scientific Computing Center, a DOE Office of Science User Facility supported by the Office of Science of the U.S. Department of Energy under Contract No. DE-AC02-05CH11231 using NERSC award BES-ERCAP0026843.

References

[1] N. Martensson and M. Erikson, *Nuclear Inst. and Meth. in Physics Research Section A: Accelerators, Spectrometers, Detectors and Associated Equipment*, **907**, 97, (2018).
[2] E.A. Seddon, et al., *Reports on Progress in Physics*, **80**, 115901, (2017).
[3] G.B. Stephenson, A. Robert, and G. Grübel, *Nature Materials*, **8**, 702, (2009).
[4] G. Grübel, G.B. Stephenson, C. Gutt, H. Sinn, and T. Tschentscher, *Nucl. Instruments and Methods: Phys. Res. Sect. B: Beam Interact. With Mater. Atoms*, **262**, 357, (2007).
[5] M. Sutton, http://www.physics.mcgill.ca/~mark/coherence/yorick/highqbeta.pdf, Oct. 24, 2024.
[6] J. Wang, https://www.aps.anl.gov/Feature-Beamlines/Coherent-Surface-Scattering-Imaging, Oct. 24, 2024.
[7] P.N. Pussey, "Statistical Properties of Scattered Radiation" in *Photon Correlation Spectroscopy and Velocimetry*, Springer, (1977).
[8] M. Sutton, *Comptes rendes – Physique*, **9**, 657, (2008).
[9] L. Mandel and E. Wolf, *Optical Coherence and Quantum Optics*, Cambridge University Press, (1995).
[10] S. Reiche, *Nuclear Inst. and Meth. in Physics Research Section A: Accelerators, Spectrometers, Detectors and Associated Equipment*, **429**, 243, (1999).